Since January 2020 Elsevier has created a COVID-19 resource centre with free information in English and Mandarin on the novel coronavirus COVID-19. The COVID-19 resource centre is hosted on Elsevier Connect, the company's public news and information website.

Biosensors and Bioelectronics 188 (2021) 113282

Contents lists available at ScienceDirect

Biosensors and Bioelectronics

journal homepage: www.elsevier.com/locate/bios

Ultrafast multiplexed detection of SARS-CoV-2 RNA using a rapid droplet digital PCR system

Hao Yin [a,b,1], Zhenhua Wu [a,1], Nan Shi [c,1], Yong Qi [d], Xiaoyu Jian [a], Lin Zhou [a], Yigang Tong [e], Zule Cheng [a,**], Jianlong Zhao [a], Hongju Mao [a,b,*]

[a] State Key Laboratory of Transducer Technology, Shanghai Institute of Microsystem and Information Technology, Chinese Academy of Sciences, Shanghai, 200050, China
[b] Center of Materials Science and Optoelectronics Engineering, University of Chinese Academy of Sciences, Beijing, 100049, China
[c] Expec-Advanced Research Center, Saudi Aramco, Dhahran, 34464, Saudi Arabia
[d] Huadong Research Institute for Medicine and Biotechniques, Nanjing, Jiangsu, 210000, China
[e] Beijing Advanced Innovation Center for Soft Matter Science and Engineering (BAIC-SM), College of Life Science and Technology, Beijing University of Chemical Technology, Beijing, 100049, China

ARTICLE INFO

Keywords:
Nucleic testing
Rapid digital PCR system
SARS-CoV-2 detection
Microfluidic technology

ABSTRACT

We report the first combination of droplet digital and rapid PCR techniques for efficient, accurate, and quantitative detection of SARS-CoV-2 RNA. The presented rapid digital PCR system simultaneously detects two specific targets (ORF1ab and N genes) and one reference gene (RNase P) with a single PCR thermal cycling period around 7 s and the total running time less than 5 min. A clear positive signal could be identified within 115 s via the rapid digital RT-PCR, suggesting its efficiency for the end-point detection. In addition, benchmark tests with serial diluted reference samples of SARS-CoV-2 RNA reveal the excellent accuracy of our system (R^2>0.99). More importantly, the rapid digital PCR system gives consistent and accurate detection of low-concentration reference samples, whereas qPCR yields Ct values with significant variations that could lead to false-negative results. Finally, we apply the rapid digital PCR system to analyze clinical samples with both positive and control cases, where results are consistent with qPCR test outcomes. By providing similar accuracy with qPCR while minimizing the detection time-consuming and the false-negative tendency, the presented rapid digital PCR system represents a promising improvement on the rapid diagnosis of COVID-19.

1. Introduction

Nucleic acid testing has been extensively used for the clinical diagnosis of the coronavirus disease 2019 (COVID-19), in which a novel coronavirus named severe acute respiratory syndrome coronavirus 2 (SARS-CoV-2) is identified as the pathogen (Wu et al., 2020; Zhou et al., 2020). In particular, real-time reverse transcription-quantitative polymerase chain reaction (RT-qPCR) is the predominant method for diagnosing COVID-19 worldwide. During the test, SARS-CoV-2 RNA in the sample is first reverse-transcribed to its complementary DNA (cDNA), of which specific regions are amplified by polymerase chain reaction (PCR) and detected by the fluorescence from the hydrolysis probes (Corman et al., 2020). Effective diagnosis of COVID-19 requires continuous efforts to reduce the PCR analysis time and increase the accuracy for samples with ultralow viral load.

Rapid PCR can be achieved by shortening the time required for individual PCR steps (i.e., denaturation, annealing, extension), reducing the ramping time (heating-and-cooling), or the combination of both. The first strategy has been demonstrated in previous studies, where the denaturation and annealing time is reduced to 1s to enable the elongation of a 200-bp sequence in less than 15 s (Wittwer et al., 1990, 1997; Wittwer and Garling, 1991). Meanwhile, various technologies have been proposed to enhance the efficiency of thermal cycling. These systems usually involve small sample volume (nL - μL) or large contacting

* Corresponding author. State Key Laboratory of Transducer Technology, Shanghai Institute of Microsystem and Information Technology, Chinese Academy of Sciences, Shanghai, 200050, China.
** Corresponding author.
E-mail addresses: chengzule@163.com (Z. Cheng), hjmao@mail.sim.ac.cn (H. Mao).
[1] Hao Yin, Zhenhua Wu and Nan Shi contributed to this work equally.

https://doi.org/10.1016/j.bios.2021.113282
Received 14 December 2020; Received in revised form 1 April 2021; Accepted 22 April 2021
Available online 4 May 2021

surface to enhance the heat exchange (Neuzil et al., 2006; Sposito et al., 2016). Besides, indirect heating methods such as infrared laser (Kim et al., 2009) and plasmonic photothermal heating (Son et al., 2015) have been developed in addition to conventional direct Joule heating (Cai et al., 2019). Particularly, microfluidic devices are fabricated to perform rapid RT-qPCR for detecting viral RNA within 30 min (Powell et al., 2018).

On the other hand, RT-qPCR could yield false negative results when the concentration of target RNA sequences is low or interfered by other sequences (Wang et al., 2020; Yu et al., 2020). Applying rapid PCR strategies with RT-qPCR would further reduce the amplification efficiency and detection sensitivity of target sequences (Fernandez-Carballo et al., 2018). Moreover, RT-qPCR tests are semi-quantitative depending on specific reagent kits and instruments so the diagnosis of COVID-19 cases could vary due to different lab facilities and operations. Although this problem could be mitigated by the introduction of international reference materials that acts as calibration standards, such standards are not yet available for all clinically important viral pathogens (Nixon et al., 2014). Therefore, based on this existing gold standard, we can also introduce more fast and accurate technique to further improve the detection performance.

Here, we develop a fast, accurate, and quantitative nucleic acid detection system for the effective diagnosis of COVID-19, by combining the concept of rapid PCR and droplet digital PCR (ddPCR) for the first time. The ddPCR part of the system is a microfluidic device that generates, splits, and stores droplets as independent reactors for amplifying target nucleic acid sequences. Because most droplets involve either single or no target sequence (Morrison et al., 2006), these sequences can be amplified un-biasedly regardless of their original concentration in the sample. In addition, quantification of target sequences is achieved via the Poisson distribution formula, which relates the number fraction of positive fluorescent droplets after amplification and the origin copy number of the target sequence (Cao et al., 2017; Majeed et al., 2012; Whale et al., 2012). Furthermore, the rapid PCR in our system is enabled by in-situ heater arrays and the small volume of the droplet-based PCR reacting system.

We start by optimizing operating parameters of rapid ddPCR with reference RNA samples, using a moderate concentration of triple target sequences, ORF1ab, N gene and RNase P gene. The performance of the optimized system is then benchmarked in testing reference RNA samples over a broad range of target sequence concentration (serial dilution). Particularly, we compare the accuracy and consistency of rapid ddRT-PCR and RT-qPCR in analyzing ultralow-viral-load reference samples. Finally, we apply the system in diagnosing clinical COVID-19 samples and compare results with commercial test kits based on RT-qPCR.

2. Material and methods

2.1. Rapid ddPCR system fabrication

The digital PCR part of the system is based on the microfluidic technology. And we use microfluidic chips to generate, split, and store droplets as independent reactors for digital PCR. Besides, the rapid PCR thermal cycling is enabled by in-suit heater arrays. The electrical elements (heaters, temperature sensors and scribe lines) of the heater array are fabricated by lift-off process, and the heating discs are made in a second lithography step (details of the heater array and the microfluidic chip fabrication process can be found in the Supplementary Material). The resistance of heaters and temperature sensors are tested using a semiconductor parameter analyzer (Keithley 4200, USA). Subsequently, the heater array is soldered onto an interface PCB (printed circuit board) (Supplementary Figure. 2c) and connected to a second PCB that monitors and controls the temperature. The second PCB consist of eight 2.5 mA constant DC sources, 12 V DC power, and other interfaces for connecting the LabVIEW Data Acquisition (DAQ) card (National Instruments, Inc. USA). Temperature sensing is performed by applying constant current to each of the eight sensor electrodes while monitoring voltage changes across the sensors. A filter circuit is adopted to acquire a stable output voltage. Before testing, the PCR device is calibrated by placing the devices in the oven equipped with a thermocouple. During calibration, the oven temperature is adjusted from 40 °C to 100 °C, while the temperature and corresponding voltage changes are collected by the DAQ card.

Thermal cycling is controlled using the PID (proportional-integral-derivative) method via LabVIEW. Briefly, the voltage changes from the temperature sensors are converted into temperature and compared with the programmed value. After processing using the PID control algorithm, generated duty cycles are converted to low-power PWM (Pulse-Width Modulation) signals, which then control the output of 12 V DC power via eight n-type MOSFETs (Metal-Oxide-Semiconductor Field Effect Transistor) to adjust the average DC power applied to heaters.

2.2. Temperature control performance

The fabricated PCR device is calibrated according to a previous report (Sposito et al., 2016). The resistance of the heaters and sensors is measured as $42 \pm 1.26\Omega$ and $405 \pm 8.1\Omega$, respectively. Numerical simulation shows uniform temperature across the reaction area (Supplementary Video 2) due to silicon's high thermal conductivity and the cut-through design of independent heating discs.

The temperature of thermal cycling is controlled by the closed-loop proportional-integral-derivative (PID) method. A 12 V power source is used for the operation of the heaters, where power pulses are converted from low-power pulse-width modulated (PWM) signals generated by the computer. Temperature sensing is performed by applying a small constant current to the sensor electrodes while monitoring the voltage difference between sensors. A current of 2.5 mA is used to prevent the Joule heating of the sensors. The voltage difference between sensors is recorded as a function of the temperature that is measured by the LabVIEW Data Acquisition (DAQ) card with a precision of ±0.05 °C.

We first test the efficiency of bare heater arrays on thermal cycling without microfluidic chips; the heater arrays it require approximately 0.3 s to reach the target temperature of 95 °C from 60 °C. The cooling time is longer by approximately 1 s. Next, we test efficiency of heaters on thermal cycling with a microfluidic chip. As thermal energy could transfer from the heater to the chip, heating and cooling rates are slower than those of the bare heaters. Moreover, owing to the small thermal conductivity coefficients of glass and PDMS (1.1 Wm^{-1} K^{-1} and 0.21 Wm^{-1} K^{-1}, respectively), heat dissipation around the heating area is minimal; thus, the heating and cooling rates are similar to those of the bare heaters, which are 0.5 s and 1.5 s, respectively. The short temperature transition times of this PCR device enable fast PCR cycle times for target DNA amplification.

When the system reaches the thermal equilibrium, the temperature of PCR mixtures inside droplets should be synchronized with that measured by temperature sensors. However, the thin glass separating the sensor and droplet storage chamber causes the delay of temperature change in PCR mixtures during the thermal cycling. To investigate the effect of this delay on the denaturation of PCR, a thin gold film temperature sensor is embedded in the droplet storage chamber to record temperature in the mineral oil filled chamber during the thermal cycling. Owing to the big surface-to-volume ratio of the chambers and the small volumes of PCR mix, the temperatures of the sensor can be seen as identical to that of the PCR mix. The temperature measured by the gold sensor in the storage chamber closely followed that from the platinum sensors next to the heater array with a dynamic offset of less than 0.5 s. In a 2-s denaturing step programmed by the heater control, the duration of the effective denaturation temperature (between 90 °C and 95 °C) is measured for approximately 1.2 s in the storage chamber (Fig. 1d), which is sufficient for the denaturation of double DNA strands (Wittwer and Garling, 1991). Therefore, the delay in temperature change due to the thin glass slide would not have dramatic effect on the

Figures:

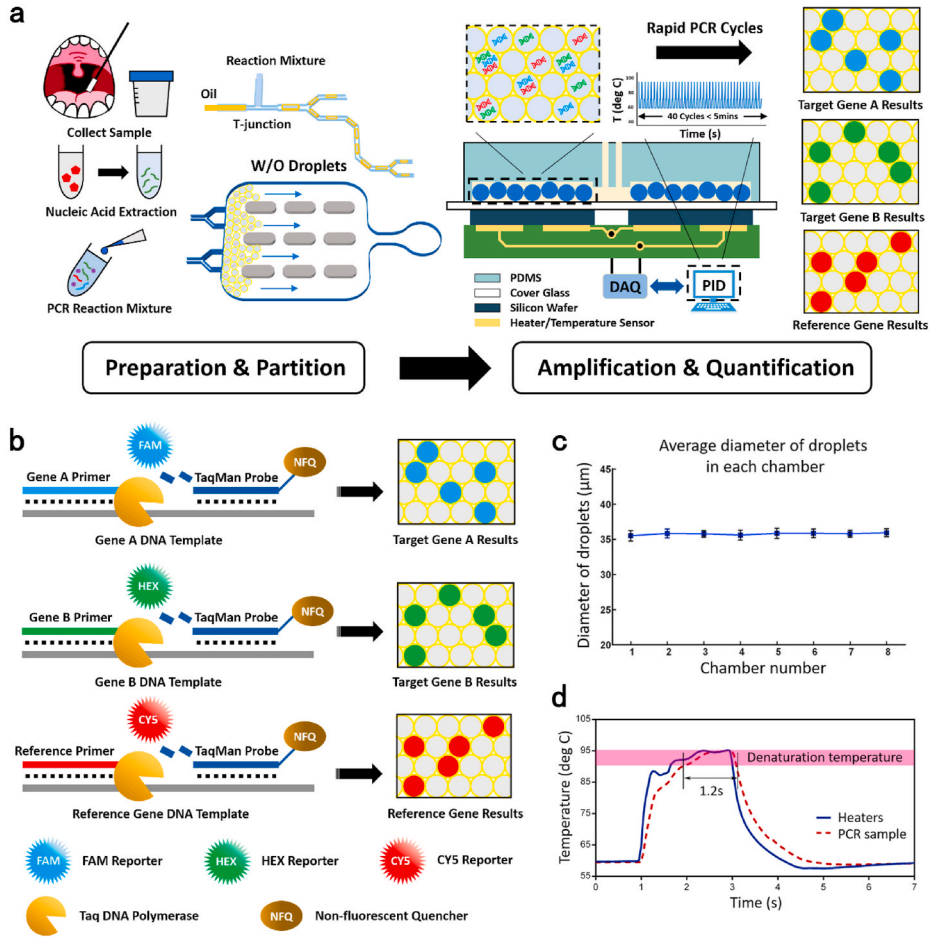

Fig. 1. Principles and characteristics of the rapid digital PCR system. (**a**) Workflow of rapid digital PCR method consists of four key steps, sample preparation, reaction mixture partition, amplification process, and targets quantification. (**b**) Hydrolysis of different TaqMan probes generates distinct positive fluorescence signals. (**c**) Average diameter of droplets in each storage chamber and error bars show the standard deviation droplet size distribution. (**d**) Thermal profile of the heater (blue line) and PCR sample (red dotted line) during an 8-s thermal cycle of 2 s at 95 °C and 6 s at 60 °C. The semi-transparent red zone represents the effective temperature range for DNA denaturation. (For interpretation of the references to colour in this figure legend, the reader is referred to the Web version of this article.)

rapid PCR process.

2.3. Reagent preparation

The RdRp gene in the open reading frame 1 ab region (ORF1ab) and the N gene from SARS-CoV-2 are selected as the specific target sequences, and RNase P gene is tested for the assessment of specimen quality. Primers and TaqMan probes for ORF1ab, N and RNase P gene are designed based on published methods from the World Health Organization (WHO), Chinese Center for Disease Control and Prevention (CCDC), and the Centers for Disease Control and Prevention (UCDC). The total RNA of saliva from the healthy is extracted using the viral RNA mini kit (QIAGEN, Germany), which contains RNase P gene sequence. The SARS-CoV-2 RNA reference material that contains ORF1ab and N gene sequence is obtained from NMIC (National Institute of Metrology, China). The concentration of ORF1ab and N gene (copies/μL) is calculated using the concentration data provided by NMIC. Then, these sequence (RNase P, ORF1ab and N gene) are mixed in the same proportion as in the initial concentration of the sample. Finally, the genomic RNA of the target sequences in SARS-CoV-2 is then diluted in series from 10 to 10^5 copies/μL using Nuclease-free water (Sangon Biotech, China).

The components of the 25-μL rapid RT-PCR mixture consist of 10 μL RNA, 5 μL of 5X reaction Buffer (250 mM Tris-HCl at pH 8.3, 375 mM KCl, and 15 mM $MgCl_2$, Thermo Fisher Scientific, USA), 1 μL of 200 U/μL M-MLV Reverse Transcriptase (Thermo Fisher Scientific, USA), 0.6 μL of 5 U/μL KAPA2G Fast HotStart DNA Polymerase (Roche, Switzerland), 0.5 μL RNasin inhibitor (Promega, USA), and 2 μL 2.5 μM dNTP (Roche, Switzerland). Optimized concentrations of primers and probes are shown in Supplementary Table 1. All oligonucleotides are synthesized and provided by Sangon Biotech (Shanghai, China).

2.4. Target gene detection

The continuous oil phase is prepared with white mineral oil (Fisher Scientific, USA), involving 3% w/w Abil EM 90 (Degussa/Goldschmidt, Germany) and 0.1% w/w Triton X-100 (Sigma-Aldrich, USA) as surfactants to stabilized water-in-oil droplets during thermal cycling. Afterwards, 1 μL prepared RT-PCR reaction mix and 4 μL oil phase are injected into two separate inlets at an equal positive pressure of 200 mbar provided by a Fluidiclab Pressure Controller (Prinzen Biomedical, China). Chambers are first filled with the oil phase to prevent air bubbles. Water-in-oil droplets are generated at the cross section of channels, split, and stored into different chambers.

Thermocycling of the microfluidic device is achieved by gently placing the microfluidic chip on the heater array. The optimized rapid RT-PCR program is initiated with a 15-s reverse transcription and a 15-s 'hot start' condition at 95 °C to activate the polymerase. This step is followed by 40 cycles of PCR, each kept at 95 °C for 1 s, 60 °C for 4 s, and 72 °C for 2 s. A consumer grade 20-megapixel digital camera (TD-HU608A; SANQTID, China) captures the movement of droplets in storage chambers during thermal cycling.

After the amplification, droplet storage chambers are examined under the 10 × magnification of an inverted microscope (Model IX51; Olympus, USA). The size of droplets is measured using a built-in image analysis software (DP Controller; Olympus). Images of all droplets in the chamber are captured under the bright field (100 ms exposure time), and the fluorescence of droplets is measured at excitation wavelengths of 485 nm, 535 nm, and 640 nm with the exposure time set to 2.8 s, 1.3 s,

and 1.5 s, respectively. ImageJ software and custom Python code are used to quantify the number fraction of fluorescent (positive) droplets. The original copy number of target sequence k is determined according to the Poisson distribution formula:

$$k = -N \ln\left(1 - \frac{n}{N}\right) \quad (1)$$

where n is the number of positive fluorescent droplets and N is the total number of droplets in all chambers. The quantification results of serial dilution samples are then compared with the concentration established by the National Institute of Metrology, China.

2.5. Sample preparation

Throat swab samples from clinical COVID-19 patients (n = 6) and healthy participants (n = 3) are obtained from the Huadong Research Institute for Medicine and Biotechnology (Nanjing, China). SARS-CoV-2 RNA is extracted from samples using the viral RNA mini kit (QIAGEN, Germany) according to the manufacturer's instruction. Informed consent is obtained from all participants prior to the sample collection. Six positive and three negative clinical nucleic acid samples are tested using RT-qPCR and rapid digital RT-PCR separately.

2.6. Clinical sample validation

To verify the presence of SARS-CoV-2, RT-qPCR is performed using a 25-μL reaction system, 10 μL of total nucleic acid, and an approved COVID-19 RT-qPCR kit (Sansure Biotech, China). Amplification is performed in the LightCycler 480 (Roche, Switzerland) using the following conditions: 1 cycle at 50 °C for 30 min, 95 °C for 1 min, and 45 cycles at 95 °C for 15 s and 60 °C for 30 s. The FAM, HEX and ROX fluorescence channels are used to detect ORF1ab, RNase P, and N, respectively. The successful amplification of all target genes and Ct values $\leq$ 40 are considered as a positive result for SARS-CoV-2 infection. A negative result is concluded in two cases, the Ct value is smaller than 40 for RNase P while greater than 40 for both ORF1ab and N, or no successful amplification is achieved. Other amplification results are considered inconclusive and a second detection is repeated.

3. Results

3.1. Design of the rapid ddPCR system

Our rapid ddPCR system (Fig. 1a) involves two key components: a microfluidic chip to handle droplets for digital PCR and a micro-heater array for rapid PCR. Starting from the droplet generation in the microfluidic chip, the PCR reaction mixture involving extracted nucleic acid samples and PCR reagents is rapidly dispersed into more than 20,000 droplets with mineral oil as the external phase. Droplets are generated using a single PCR sample inlet and oil inlet feeding into T-conjunctions on both sides of the chip (Thorsen et al., 2001) (Supplementary Figure. 1a). Parent droplets are formed and then passed through the splitter (Chaudhury et al., 2014), where the parent droplet is split equally to into 16 daughter droplets. The structure of the droplet splitter ensures a similar number of droplets entering each chamber and increases the droplet-generation rate.

The storage compartment in the microfluidic device involves eight independent, small chambers to enhance the efficiency of thermal cycling. Each chamber is 2 mm × 2 mm with curved corners to prevent air bubbles during oil filling. In addition, narrow and long channels between droplet splitters provide large flow resistance to prevent droplet flow back. Therefore, droplets enter the storage chamber and remain inside stably. After filling eight chambers with more than 20,000 droplets in less than 2 min, the average diameter of droplets in the chamber is measured to be 35.7 μm with the coefficient of variation (CV) smaller than 3% within and among chambers, respectively (Fig. 1c).

Each of these storage chambers has its dedicated heating disc that is 2.2 mm long and 2.0 mm wide. These heating discs are deposited on the silicon substrate and separated from the droplet storage chamber by 170-μm thin glass slip to prevent cross-contamination. Due to the low thermal mass and large surface-to-volume ratio of each disc, heater arrays apply fast temperature changes during the thermal cycling of PCR. Temperature sensors are also involved close to heater arrays for temperature control during the thermal cycling (Supplementary Figure. 2a). Both heaters and sensors are made of platinum for its linear temperature coefficient of resistance in the PCR temperature range.

Only droplets with targets sequences undergo PCR cycles, where specific fluorescent probes are cut off by the DNA polymerase and emit fluorescence that increase with PCR cycles. A charge-coupled device (CCD) is used to analyze the end-point fluorescent signal of PCR, where the number fraction of fluorescent droplets is determined and used to calculate the copy number of target sequences via the Poisson distribution formula (Whale et al., 2012). By involving different fluorescent probes targeting different gene sequences, our rapid digital PCR system allows simultaneous detection of multiple targets with a single PCR test (schematic diagram shown in Fig. 1b).

3.2. Optimizing parameters of rapid ddRT-PCR

We start by determining the time duration for reverse transcription and pre-denaturation before PCR. In droplet digital PCR, each droplet has sufficient components for the amplification of single or multiple target sequences. Its small thermal mass also allows quick response to heat conduction. We therefore reduce the reverse transcription time from 5 min (commonly used by RT-qPCR) to 10 s while maintaining the temperature at 43 °C. This reduction in time does not significantly change the number of positive droplets after PCR (Supplementary Figure. 3). Similar results also occur when the pre-denaturation time is reduced from 1 min to 10 s while the temperature is maintained at 95 °C. These results confirm that reverse transcription and pre-denaturation can finish quickly in our droplet reaction system. By adding extra 5 s to ensure the system's thermal equilibration, we set both reverse transcription and pre-denaturation time to 15 s.

Next, we use SARS-CoV-2 reference samples with target RNA sequence at 10^3 copies/μL to optimize PCR reaction parameters. This concentration value ensures the similarity of the normal viral load in most general COVID-19 patients (Wolfel et al., 2020; Zou et al., 2020).

The extension rate (including the probe decomposition) of KAPA2G Fast HS DNA Polymerase is reported as 40 bp/s at 50 °C and 155 bp/s at 75 °C (Furutani et al., 2016; Montgomery et al., 2013). Considering the length of our target sequences (ORF1ab 100bp,N gene 99bp, RNase P 65bp), the extension time at 72 °C is set to 1s.

Based on our experience, the starting point for optimizing the denaturation time at 95 °C and annealing time at 60 °C is 3s and 5s, respectively. And the total number of cycles is selected as 40. By fixing the total cycle number and the annealing time (5s), we gradually reduce the denaturation time to 1s and find this is sufficient for detecting clear positive droplets. Similarly, using the total cycle number (40) and updated denaturation time (1s), we then find 3-s annealing time can yield good results (Fig. 2a). This completes optimized parameters of PCR as: 95 °C/1 s for denaturation, 60 °C/3 s for annealing, 72 °C/1 s for extension, and the total number of cycles 40.

Notice that this optimization is conducted with a moderate concentration (10^3 copies/μL) of target sequences in the sample. On the other hand, uneven fluorescent intensity for ORF1ab among droplets arises when the concentration of all target sequences in the sample is higher than 5000 copies/μL (Supplementary Figure. 4a). This non-uniform intensity could be attributed to the competition among multiple target sequences in high-concentration samples, especially when multiple target sequences are dispersed in the same droplet. Therefore, when testing concentrated samples, annealing time and extending time are increased to 6 s and 3 s, respectively. These parameters lead to uniform

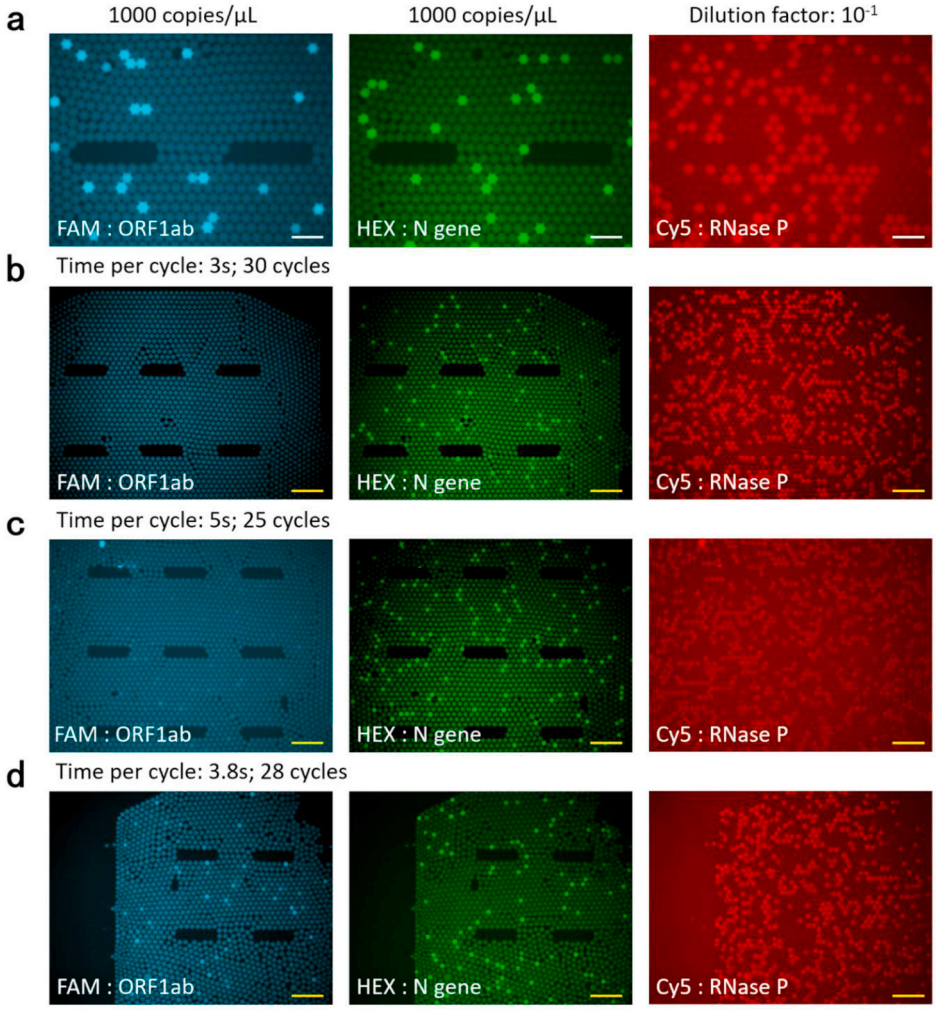

Fig. 2. Optimization of process parameters for rapid digital RT-PCR. (**a**) Fluorescent signals in microfluidic chip are obtained using three fluorescence excitation channels: excitation wavelengths of 485 nm (FAM), 535 nm (HEX), 640 nm (Cy5) for ORF1ab, N gene, RNase P, respectively. Positive signals of ORF1ab are missing when performing rapid digital RT-PCR for 30 cycles with a cycle time of 3s (**b**) and 25 cycles with a cycle time of 5s (**c**). (**d**) Positive signals of all targets are detected after 28 cycles with a cycle time of 2.8s. All experiments are performed at least 3 times. Scale bars, 100 μm (red) and 250 μm (yellow). (For interpretation of the references to colour in this figure legend, the reader is referred to the Web version of this article.)

fluorescence in all positive droplets (Supplementary Figure. 4b).

Because the COVID-19 diagnosis yields essentially a "positive" or "negative" result, we postulate that the detection time for positive signals could be reduced by providing sufficient PCR reagents in droplets. The duration of a single PCR cycle and the total number of cycles are further reduced to realize extreme fast diagnosis of COVID-19 within 2 min. While fixing total PCR cycles and the duration for denaturing and extension, we find that the annealing time can be further reduced to 2 s. In addition, positive droplets of ORF1ab only appear clearly after at least 25 PCR cycles (Fig. 2b and c). Moreover, the denaturing time is reduced from 1 s to 0.8 s without losing the detection capability. Finally, the total duration of reverse transcription (43 °C/4s) and pre-denaturation (95 °C/4s) is reduced to 8 s that can still yield reliable end-point detection results. Altogether, our rapid droplet digital PCR system can return "positive" or "negative" diagnosis of COVID-19 within 2 min, involving 28 PCR cycles and each cycle includes 95 °C/0.8 s for denaturation, 60 °C/2 s for annealing, 72 °C/1 s for extension (Supplementary Figure. 5). This analysis is faster than most present systems (Udugama et al., 2020).

3.3. *Benchmarking the sensitivity and accuracy of rapid ddRT-PCR on detecting serial diluted reference samples*

The undiluted reference sample is prepared by mixing the SARS-CoV-2 RNA Reference material from NIMM (National Institute of Metrology, China) and total RNA extracted from saliva. The concentration of ORF1ab and N gene in this undiluted sample are both 10^4 copies/μL, respectively. Serial dilution of this sample is made with different dilution factors (10^{-3}, 5×10^{-3}, 10^{-2}, 10^{-1}, 5×10^{-1}), which correspond to the concentration of SARS-CoV-2 target sequences (ORF1ab and N gene) at 10, 50, 100, 1000, and 5000 copies/μL. The concentration of RNase P in the undiluted sample is unknown so its concentration in serial diluted samples is evaluated by the dilution factor.

Each sample is tested three times for the amplification of target sequences, undergoing a 15-s reverse transcription, 15-s pre-denaturation, and 40 cycles of PCR. Each PCR cycle takes 7s, involving denaturation for 1 s, annealing for 4 s, and extension for 2 s. Droplets are then imaged using fluorescence microscopy under separate fluorescence channels, from which the number fraction of positive droplets for each target sequence is determined. Finally, this number fraction is used to compute the concentration of individual target sequences in the sample via the Poisson distribution formula (Supplementary Figure. 6).

Positive droplets under separate fluorescence channels distribute uniformly in each chamber, indicating similar PCR efficiency for both ORF1ab and N gene sequences through all droplets. More importantly, the concentration of these two target sequences predicted by rapid ddRT-PCR agrees well with that calculated from the dilution factor ($R^2 > 0.99$ for the Pearson correlation, Fig. 3a and Fig. 3b). For the reference gene RNase P, because its absolute concentration in the sample not known, we plot the detected copy number against the dilution factor used in preparing the specific sample, which also indicates good linear correlation ($R^2 = 0.9996$, Fig. 3c).

These results demonstrate the efficiency, accuracy, and sensitivity of our rapid digital PCR system for detecting specific targets (ORF1ab and

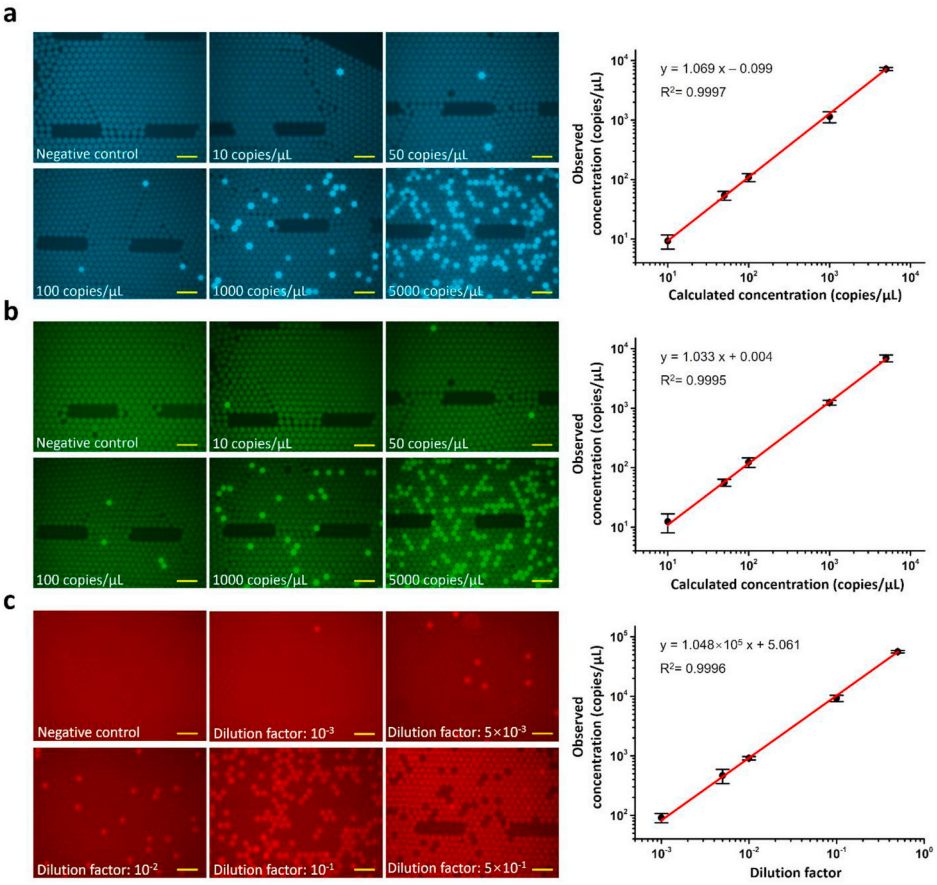

Fig. 3. Testing serial diluted SARS-CoV-2 RNA Reference Sample by rapid digital RT-PCR. (a) & (b) & (c) In the right column, fluorescence images of droplets in the reaction chamber after PCR. Concentration of templates are no template, 10, 50, 100, 1000, 5000 copies/μL for (ORF1ab & N gene in **(a) & (b)**. And the dilution factor of 10^{-3}, 5×10^{-3}, 10^{-2}, 10^{-1}, 5×10^{-1} is used to mark the concentration of the reference gene in each sample **(c)**. No positive droplets are observed in negative control samples. Correlation between detected target concentration and actual concentration calculated by the dilution factor. In the left column, R^2>0.99 in **(a) & (b)** and $R^2 = 0.9996$ in **(c).** Error bars represent the standard deviation based on at least 3 replicates of each experiment. Scale bars are 100 μm.

N gene) of SARS-CoV-2 and reference gene (RNase P). Notably, a single test completed within 5 min yields accurate results for a broad range of sample concentration that could be as low as 10 copies/μL.

3.4. Comparing rapid ddRT-PCR and RT-qPCR in detecting low-concentration standard samples

The same serial diluted reference samples used for benchmarking rapid ddPCR system are tested with RT-qPCR. The sample concentration is indicted by the Ct value (Fig. 4a). RT-qPCR yields accurate results for negative samples and diluted reference solutions with high viral load (>10 copies/test), where Ct linearly correlates with the concentration (copies/test) in the log scale ($R^2 > 0.99$, Supplementary Figure. 7).

We further compare the performance of RT-qPCR and rapid ddRT-PCR in detecting low-viral-load samples. 10 repeated tests of these two methods are performed separately for diluted reference samples, where the concentration of target sequences is 10 copies/test and 5 copies/test (Fig. 4b and c). While both methods yield positive signals for tested low-viral-load samples, detection results from RT-qPCR (Ct values) have more significant variations that are possibly due to inconsistent amplification efficiency. Such variations often lead to false-negative results that are undesired in the diagnosis of COVID-19 (Fig. 4d).

By contrast, rapid digital RT-PCR results correctly predict 3.8 copies/test and 9.4 copies/test for two low-viral-load samples, respectively (Fig. 4e). These values are slightly smaller than actual ones (calculated by the dilution factor), which could be caused by the degradation of the RNA templates during serial dilution (Fleige et al., 2006). And the relative uncertainly of digital PCR would increase as the random distribution of the template molecules number during serial dilution. This could be another reason for the deviation from the calculated concentration (Bhat et al., 2009; Zhu et al., 2014). However, this is unlikely to occur in clinical diagnosis that usually does not involve sample dilution. These results demonstrate that quantitative and un-biased PCR amplification in the rapid ddPCR system enable accurate detection of low-viral-load samples.

3.5. Detection of SARS-CoV-2 nucleic acids from clinical samples

After benchmarking the performance of rapid ddRT-PCR with reference samples, we apply this system to test clinical nucleic acid samples collected for the diagnosis of COVID-19, which involve six positive and three negative cases. The rapid ddPCR system simultaneously targets three specific sequences, ORF1ab, N and RNase P gene, and detect their copy numbers in each sample (Fig. 5a and Fig. 5b, calculated concentration is listed in Supplementary Table 2). Meanwhile, RT-qPCR is performed for the same clinical samples in the LightCycler 480 (Roche, Switzerland) using an approved RT-qPCR kit (Sansure Biotech, China).

Noticeably, rapid ddRT-PCR correctly diagnose all positive and negative cases of COVID-19 samples. In addition to qualitative results (positive or negative), rapid ddRT-PCR also provide the copy number of target sequences in each sample, which correlate linearly with the corresponding Ct value from RT-qPCR (Fig. 5b). Furthermore, rapid ddRT-PCR yields these accurate results within 10 min, whereas the standard RT-qPCR analysis takes at least 2 h.

4. Discussion

Unbiased amplification of nucleic acid sequences is important for PCR-based diagnosis of low-viral-load samples. In conventional RT-qPCR, a wide variety of nucleic acid sequences are mixed together in

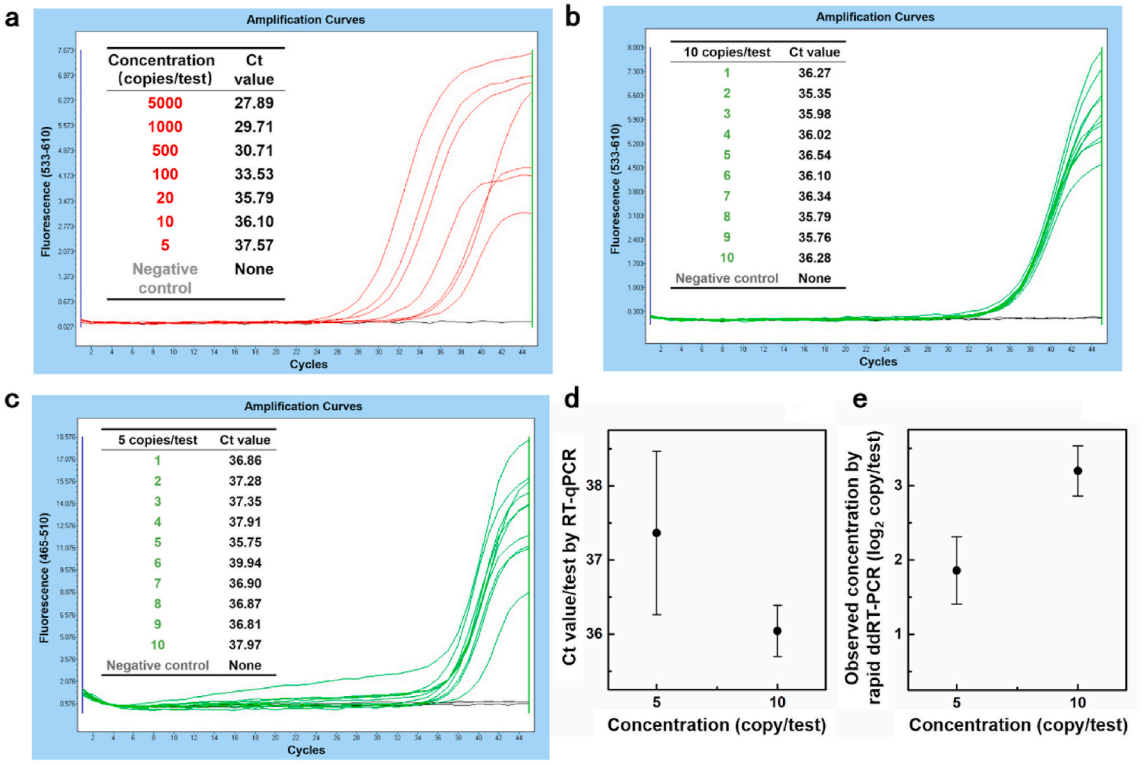

Fig. 4. Comparing results of detecting SARS-CoV-2 RNA Reference Sample using RT-qPCR and rapid digital RT-PCR. (**a**) Amplification curves and Ct values from RT-qPCR for serial diluted reference samples with the concentration of targeted N gene at 5, 10, 20, 100, 500, 1000, 5000 copies/test. **(b) & (c)** Ten detection amplification curves and Ct values for low-copy concentration samples with concentration of (**b**) 10 copies/test (target: N) and (**c**) 5 copies/test (target: ORF1ab) by RT-qPCR. (**d**) Ct values from 10 replicated testing of low-concentration reference samples using RT-qPCR. By definition, Ct scales inversely with the log-scale concentration of the target gene in the sample. (**e**) Accuracy of testing the low-concentration reference samples by rapid digital RT-PCR (10 replicated tests). To enable direct comparison with the result by RT-qPCR, the detected concentration in plotted in the log scale. Error bars represent the standard deviation based on 10 replicated testing.

the PCR tube so amplification of sequences with higher concentration is favored. Considering current efforts to detect COVID-19, samples with low concentration of targeted sequences are possible when patients are at the early-stage patients or improper sampling/processing introduces contaminants. False-negative diagnosis of these samples is highly undesired. We show this tendency by applying RT-qPCR to detect SARS-CoV-2 RNA Reference materials with extremely low concentration of target sequences (5 and 10 copies per test), where Ct values from repeated tests show a significant variation.

By contrast, the rapid ddPCR system utilizes digital droplet PCR that unbiasedly amplify target sequences regardless of their concentration in the sample. The underlying mechanism is to disperse nucleic acid sequences into individual droplets such that each droplet contains either one or no target nucleic acid sequence. Subsequent PCR ensures equal and independent amplification of all target nucleic acid sequences. Due to this property, ddPCR yields accurate results when detecting ultra-low reference samples and shows better consistence compared with RT-qPCR. Moreover, the accuracy of rapid ddPCR over a broad range of sequence concentration is verified with serial diluted reference samples. Furthermore, rapid ddRT-PCR gives consistent diagnosis of clinical COIVD-19 samples with that from commercial RT-qPCR procedures.

The second advantage of ddPCR is the capability to quantitatively measure the copy number of target nucleic acid sequences without calibration curves. Targeting specific sequences with fluorescent probes is achieved by designing suitable sequence fragments based on the principle of base complementary pairing. After completing PCR, the copy number of these target sequences is quantified with the Poisson distribution formula, where the final number of fluorescent or positive drops (n) is related with the copy number (k) of the specific target sequence as (1) given the total number of droplets N. Because all target nucleic acid sequences are amplified, simultaneous detection of different target sequences is possible. When applying our rapid ddRT-PCR in the diagnosis of COVID-19 (reference and clinical samples), ORF1ab, N and RNase P gene are selected as the target sequences based on previous guidelines for COVID-19 diagnosis (Corman et al., 2020; Liu et al., 2020). Quantitative results from rapid ddRT-PCR are consistent with both specific targets at known concentration and dilution ratio of reference genes with unknown concentration.

This quantification capability benefits the diagnosis of COVID-19 in different ways. First, compared with semi-quantitative RT-qPCR, rapid ddPCR yields more consistent results that enable global criteria of diagnosing positive COVID-19 cases. In addition, quantitative results could reduce the analysis time by avoiding the second test that is often required by RT-qPCR due to its indecisiveness. Finally, although current diagnosis mostly focuses on the qualitative result (positive or negative), quantitative detection of the viral copy number is important for long-term monitoring of patients' recovery or evaluating the performance of medicines or vaccines.

Last but not least, we have optimized operating parameters of the rapid ddPCR system to significantly reduce the analysis time. While routine RT-qPCR takes hours to days to yield results due to the relatively large reaction volume, rapid ddRT-PCR is able to give accurate and quantitative results within 15 min including the sample preparation. If only qualitative results are desired, rapid ddRT-PCR can diagnose positive or negative cases in less than 2 min, which is a remarkable improvement over RT-qPCR.

Reducing the analysis time of rapid ddPCR is enabled by both in-situ heater arrays and the droplet-based PCR system. First, in-situ heater arrays and small PCR reaction volume (22.4 pL per droplet) ensures rapid thermal cycling. For example, we are able to reduce pre-

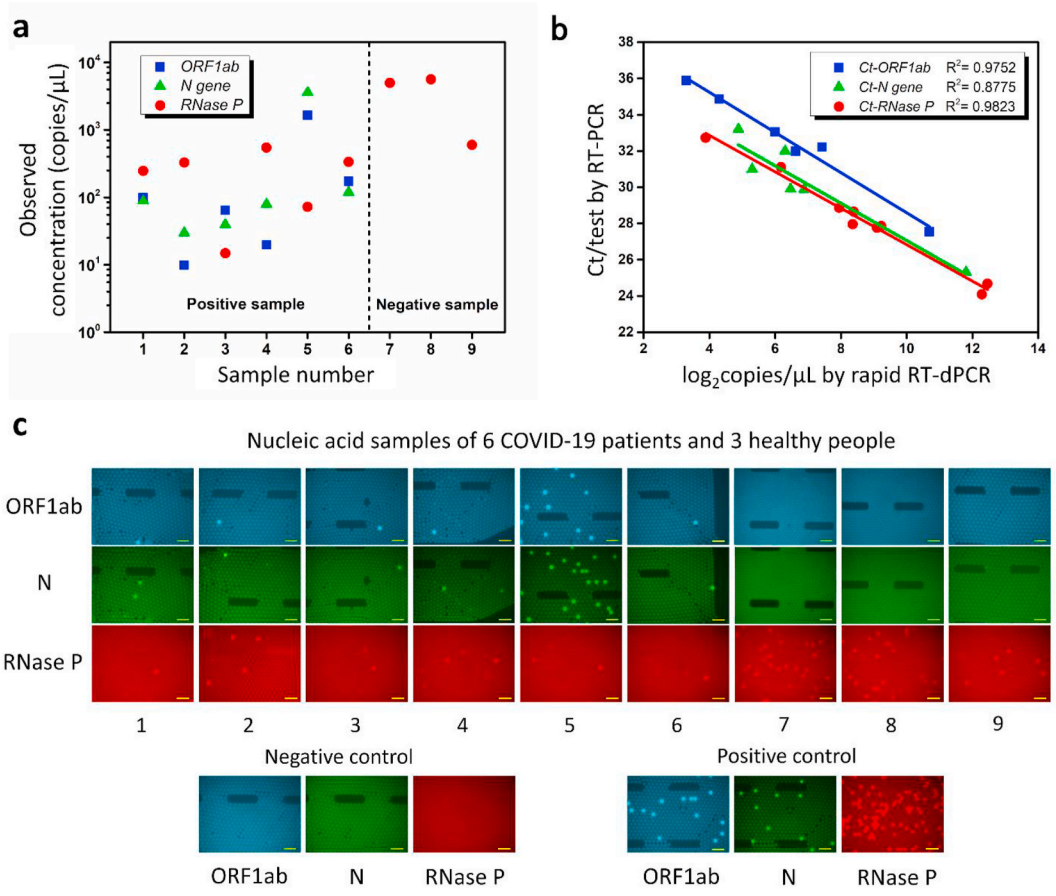

Fig. 5. Quantitative analysis of ORF1ab, N gene, and RNase P in clinical samples. (**a**) Detected copy number of three target sequences in 9 nucleic acid samples by rapid digital RT-PCR. (**b**) Ct values from RT-qPCR are plotted against the target copy number acquired by rapid digital PCR. (**c**) Fluorescence images showing the test results of nucleic acid samples from rapid digital RT-PCR. Top, 9 clinic samples. Bottom, negative (RNAse-free water, Sangon Biotech) and positive (SARS-CoV-2 genomic RNA reference, National Institute of Metrology, China) control samples. Scale bars, 100 μm.

denaturation and reverse transcription from 6 min to 30 s. Similarly, each PCR cycle time is reduced to 7 s. More importantly, the reduction of analysis time does not compromise the accuracy or sensitivity of our rapid ddPCR system, whereas the opposite has been suggested for qPCR involving rapid PCR techniques (Fernandez-Carballo et al., 2018). The key fact enabling fast digital PCR is the presence of single target RNA sequence in each droplet-based reaction unit. Sufficient chemical reagents and independent environment thus ensures the amplification of target sequences.

5. Conclusion

In summary, we demonstrate the efficiency and accuracy of the rapid ddPCR system based on droplet microfluidics for digital PCR and in-situ heater arrays for efficient thermal cycling. Quantitative and accurate detection of COVID-19 target sequence concentration (copy number) in serial diluted reference samples is achieved via a 5-min ddRT-PCR process which demonstrates the feasibility of using ddPCR for rapid detection of SARS-CoV-2. Particularly, rapid ddRT-PCR results showed outstanding consistency for sequence concentration as low as 5 copies/test. Furthermore, applying rapid ddRT-PCR in the diagnosis of clinical COVID-19 samples yields consistent results with commercial RT-qPCR kits but requires much less analysis time. We envision that these advantages of rapid ddRT-PCR not only enable more efficient detection of COVID-19 cases, but also improve the monitoring of patient recovery as well as the evaluation of medicines or vaccines for COVID-19.

CRediT authorship contribution statement

Hao Yin: Methodology, Visualization, Writing – original draft. **Zhenhua Wu:** Methodology, Writing – review & editing, Investigation. **Nan Shi:** Validation, Writing – review & editing. **Yong Qi:** Resources. **Xiaoyu Jian:** Investigation. **Lin Zhou:** Formal analysis. **Yigang Tong:** Resources. **Zule Cheng:** Conceptualization, Methodology. **Jianlong Zhao:** Funding acquisition. **Hongju Mao:** Supervision, Project administration, Funding acquisition.

Declaration of competing interest

The authors declare that they have no known ompeting financial interests or personal relationships that could have appeared to influence the work reported in this paper.

Acknowledgments

This study was supported by Grants from National Key Research and Development Program, China (No.2018YFA0108202 and 2017YFA0205300), National Science Foundation, China (No. 61971410, 61701171, 61801464 and 61801465).

Appendix A. Supplementary data

Supplementary data to this article can be found online at https://doi.org/10.1016/j.bios.2021.113282.

References

Bhat, S., Herrmann, J., Armishaw, P., Corbisier, P., Emslie, K.R., 2009. Single molecule detection in nanofluidic digital array enables accurate measurement of DNA copy number. Anal. Bioanal. Chem. 394, 457–467.

Cai, Q., Fauvart, M., Wiederkehr, R.S., Jones, B., Cools, P., Goos, P., Vaneechoutte, M., Stakenborg, T., 2019. Ultra-fast, sensitive and quantitative on-chip detection of group B streptococci in clinical samples. Talanta 192, 220–225.

Cao, L., Cui, X., Hu, J., Li, Z., Choi, J.R., Yang, Q., Lin, M., Ying Hui, L., Xu, F., 2017. Advances in digital polymerase chain reaction (dPCR) and its emerging biomedical applications. Biosens. Bioelectron. 90, 459–474.

Chaudhury, M.K., Chakrabarti, A., Tibrewal, T., 2014. Coalescence of drops near a hydrophilic boundary leads to long range directed motion. Extreme Mechanics Letters 1, 104–113.

Corman, V.M., Landt, O., Kaiser, M., Molenkamp, R., Meijer, A., Chu, D.K., Bleicker, T., Brunink, S., Schneider, J., Schmidt, M.L., Mulders, D.G., Haagmans, B.L., van der Veer, B., van den Brink, S., Wijsman, L., Goderski, G., Romette, J.L., Ellis, J., Zambon, M., Peiris, M., Goossens, H., Reusken, C., Koopmans, M.P., Drosten, C., 2020. Detection of 2019 novel coronavirus (2019-nCoV) by real-time RT-PCR. Euro Surveill. 25.

Fernandez-Carballo, B.L., McBeth, C., McGuiness, I., Kalashnikov, M., Baum, C., Borros, S., Sharon, A., Sauer-Budge, A.F., 2018. Continuous-flow, microfluidic, qRT-PCR system for RNA virus detection. Anal. Bioanal. Chem. 410, 33–43.

Fleige, S., Walf, V., Huch, S., Prgomet, C., Sehm, J., Pfaffl, M.W., 2006. Comparison of relative mRNA quantification models and the impact of RNA integrity in quantitative real-time RT-PCR. Biotechnol. Lett. 28, 1601–1613.

Furutani, S., Naruishi, N., Hagihara, Y., Nagai, H., 2016. Development of an on-site rapid real-time polymerase chain reaction system and the characterization of suitable DNA polymerases for TaqMan probe technology. Anal. Bioanal. Chem. 408, 5641–5649.

Kim, H., Vishniakou, S., Faris, G.W., 2009. Petri dish PCR: laser-heated reactions in nanoliter droplet arrays. Lab Chip 9, 1230–1235.

Liu, X., Feng, J., Zhang, Q., Guo, D., Zhang, L., Suo, T., Hu, W., Guo, M., Wang, X., Huang, Z., Xiong, Y., Chen, G., Chen, Y., Lan, K., 2020. Analytical comparisons of SARS-COV-2 detection by qRT-PCR and ddPCR with multiple primer/probe sets. Emerg. Microb. Infect. 9, 1175–1179.

Majeed, B., Jones, B., Tezcan, D.S., Tutunjyan, N., Haspeslagh, L., Peeters, S., Fiorini, P., Op de Beeck, M., Van Hoof, C., Hiraoka, M., Tanaka, H., Yamashita, I., 2012. Silicon based system for single-nucleotide-polymorphism detection: chip fabrication and thermal characterization of polymerase chain reaction microchamber. Jpn. J. Appl. Phys. 51.

Montgomery, J.L., Rejali, N., Wittwer, C.T., 2013. Stopped-flow DNA polymerase assay by continuous monitoring of dNTP incorporation by fluorescence. Anal. Biochem. 441, 133–139.

Morrison, T., Hurley, J., Garcia, J., Yoder, K., Katz, A., Roberts, D., Cho, J., Kanigan, T., Ilyin, S.E., Horowitz, D., Dixon, J.M., Brenan, C.J.H., 2006. Nanoliter high throughput quantitative PCR. Nucleic Acids Res. 34.

Neuzil, P., Zhang, C., Pipper, J., Oh, S., Zhuo, L., 2006. Ultra fast miniaturized real-time PCR: 40 cycles in less than six minutes. Nucleic Acids Res. 34, e77.

Nixon, G., Garson, J.A., Grant, P., Nastouli, E., Foy, C.A., Huggett, J.F., 2014. Comparative study of sensitivity, linearity, and resistance to inhibition of digital and nondigital polymerase chain reaction and loop mediated isothermal amplification assays for quantification of human cytomegalovirus. Anal. Chem. 86, 4387–4394.

Powell, L., Wiederkehr, R.S., Damascus, P., Fauvart, M., Buja, F., Stakenborg, T., Ray, S. C., Fiorini, P., Osburn, W.O., 2018. Rapid and sensitive detection of viral nucleic acids using silicon microchips. Analyst 143, 2596–2603.

Son, J.H., Cho, B., Hong, S., Lee, S.H., Hoxha, O., Haack, A.J., Lee, L.P., 2015. Ultrafast photonic PCR. Light Sci. Appl. 4.

Sposito, A., Hoang, V., DeVoe, D.L., 2016. Rapid real-time PCR and high resolution melt analysis in a self-filling thermoplastic chip. Lab Chip 16, 3524–3531.

Thorsen, T., Roberts, R.W., Arnold, F.H., Quake, S.R., 2001. Dynamic pattern formation in a vesicle-generating microfluidic device. Phys. Rev. Lett. 86, 4163–4166.

Udugama, B., Kadhiresan, P., Kozlowski, H.N., Malekjahani, A., Osborne, M., Li, V.Y.C., Chen, H., Mubareka, S., Gubbay, J.B., Chan, W.C.W., 2020. Diagnosing COVID-19: the disease and tools for detection. ACS Nano 14, 3822–3835.

Wang, Y., Kang, H., Liu, X., Tong, Z., 2020. Combination of RT-qPCR testing and clinical features for diagnosis of COVID-19 facilitates management of SARS-CoV-2 outbreak. J. Med. Virol. 92, 538–539.

Whale, A.S., Huggett, J.F., Cowen, S., Speirs, V., Shaw, J., Ellison, S., Foy, C.A., Scott, D. J., 2012. Comparison of microfluidic digital PCR and conventional quantitative PCR for measuring copy number variation. Nucleic Acids Res. 40.

Wittwer, C.T., Fillmore, G.C., Garling, D.J., 1990. Minimizing the time required for DNA amplification by efficient heat-transfer to small samples. Anal. Biochem. 186, 328–331.

Wittwer, C.T., Garling, D.J., 1991. Rapid cycle DNA amplification - time and temperature optimization. Biotechniques 10, 76-+.

Wittwer, C.T., Ririe, K.M., Andrew, R.V., David, D.A., Gundry, R.A., Balis, U.J., 1997. The LightCycler(TM) a microvolume multisample fluorimeter with rapid temperature control. Biotechniques 22, 176–181.

Wolfel, R., Corman, V.M., Guggemos, W., Seilmaier, M., Zange, S., Muller, M.A., Niemeyer, D., Jones, T.C., Vollmar, P., Rothe, C., Hoelscher, M., Bleicker, T., Brunink, S., Schneider, J., Ehmann, R., Zwirglmaier, K., Drosten, C., Wendtner, C., 2020. Virological assessment of hospitalized patients with COVID-2019. Nature 581, 465.

Wu, F., Zhao, S., Yu, B., Chen, Y.M., Wang, W., Song, Z.G., Hu, Y., Tao, Z.W., Tian, J.H., Pei, Y.Y., Yuan, M.L., Zhang, Y.L., Dai, F.H., Liu, Y., Wang, Q.M., Zheng, J.J., Xu, L., Holmes, E.C., Zhang, Y.Z., 2020. A new coronavirus associated with human respiratory disease in China. Nature 579, 265.

Yu, F., Yan, L., Wang, N., Yang, S., Wang, L., Tang, Y., Gao, G., Wang, S., Ma, C., Xie, R., Wang, F., Tan, C., Zhu, L., Guo, Y., Zhang, F., 2020. Quantitative detection and viral load analysis of SARS-CoV-2 in infected patients. Clin. Infect. Dis.

Zhou, P., Yang, X.L., Wang, X.G., Hu, B., Zhang, L., Zhang, W., Si, H.R., Zhu, Y., Li, B., Huang, C.L., Chen, H.D., Chen, J., Luo, Y., Guo, H., Jiang, R.D., Liu, M.Q., Chen, Y., Shen, X.R., Wang, X., Zheng, X.S., Zhao, K., Chen, Q.J., Deng, F., Liu, L.L., Yan, B., Zhan, F.X., Wang, Y.Y., Xiao, G.F., Shi, Z.L., 2020. A pneumonia outbreak associated with a new coronavirus of probable bat origin. Nature 579, 270–273.

Zhu, Q., Qiu, L., Yu, B., Xu, Y., Gao, Y., Pan, T., Tian, Q., Song, Q., Jin, W., Jin, Q., Mu, Y., 2014. Digital PCR on an integrated self-priming compartmentalization chip. Lab Chip 14, 1176–1185.

Zou, L.R., Ruan, F., Huang, M.X., Liang, L.J., Huang, H.T., Hong, Z.S., Yu, J.X., Kang, M., Song, Y.C., Xia, J.Y., Guo, Q.F., Song, T., He, J.F., Yen, H.L., Peiris, M., Wu, J., 2020. SARS-CoV-2 viral load in upper respiratory specimens of infected patients. N. Engl. J. Med. 382, 1177–1179.